A&A 412, 293–304 (2003)
DOI: 10.1051/0004-6361:20031413

Astronomy & Astrophysics

Coronal Mass Ejection (CME)-induced shock formation, propagation and some temporally and spatially developing shock parameters relevant to particle energization

B. Tsurutani[1], S. T. Wu[2], T. X. Zhang[2], and M. Dryer[3]

[1] Jet Propulsion Laboratory, California Institute of Technology Pasadena, CA, USA
[2] Center for Space Plasma and Aeronomic Research The University of Alabama in Huntsville, Huntsville, AL 35899, USA
[3] NOAA Space Environment Center, 325 Broadway, Boulder, CO 80305, USA

Received 10 June 2003 / Accepted 11 September 2003

Abstract. Interplanetary shocks accelerate solar energetic particles (SEPs) from the point of shock formation in the lower corona, and continuously as the shock propagates outward to 1 AU and beyond. In this study, the formation properties of a CME-induced shock and propagation characteristics are studied from the inner corona to 1 AU. We use a 2D, three-component (i.e., 2.5D), time-dependent MHD code in our model. A well-studied CME event (the 1997 January 6−12 Sun-Earth Connection Event) is used as a baseline for this study. The solar wind conditions measured at 1 AU (WIND data) are used to motivate our effort to model the CME driven shock. It is found that the fast forward shock forms originally at ~3.2 R_s (solar radii) from the solar surface in the ecliptic plane for the assumed CME and background solar wind parameters. In our model, this occurs ~2 hrs after CME initiation. The shock formation at higher (~30°) latitudes measured from the ecliptic plane is further from the Sun (~3.6 R_s) because of higher local magnetosonic speeds that must be exceeded by the original disturbance for shock formation. Finally, the shock becomes symmetric at 16 R_s. In the ecliptic plane at 16 R_s the fast shock Mach number (M_f) is ~3.5, and at 30° latitude, $M_f \sim 1.7$, considerably weaker. A maximum in the fast shock Mach number of 4 is reached at 130 R_s in the ecliptic plane. The M_f decreases to 3.5 by 1 AU. Other properties of the shock, as well as its relationship to the local interplanetary properties through which it passes, are discussed. The interplanetary counterpart, ICME, of the coronal CME, is also discussed. These shock properties, we believe, are relevant to the shock's ability to accelerate particles to energies as high as 100 MeV. The actual physical process, however, is not discussed in this paper.

Key words. Sun: corona – Sun: interplanetary shocks – Sun: CME – Sun: MHD

1. Introduction

There are two types of solar flare particle events: 1) "impulsive" events that have a short duration of a few minutes in which the particles propagate to 1 AU within tens of minutes (after visible X-ray and disc flaring at the Sun), and 2) "gradual" events that have much longer onset times and are delayed from the prompt event onset by hours (Cane et al. 1986; Lin 1987; Kallenrode 1993; Reames 1995; Heras et al. 1995). One possible explanation of the two types of events has to do with magnetic connectivity to the particle acceleration site. Eastern flares may have prompt responses of highly energetic particles at 1 AU. These events, then, may be followed by delays until the expanding shocks connect with the observer via the interplanetary magnetic field (IMF) for energization of the lower energy particles (say, ≤50 MeV). In this sense, the latter, gradual events are delayed by hours from the prompt events. Alternatively, onsets in gradual events from well-connected IMF flare sources in the western hemisphere can be as fast as in impulsive ones compared to onset in microwaves/X-rays and/or some other flare signatures (Kallenrode 1993; Lario et al. 1998). Later in this paper, we will offer a scenario explaining this latter effect.

Of these two types, the gradual events are the most intense (Kahler 1984; Reames 1999) and of greater danger in radiation (space weather) effects. For instance, the energetic particles can cause spacecraft solar panel degradation, single event upsets (SEUs) in the electronics, and can pose other radiation hazards as well. The gradual events are believed to be accelerated at coronal/interplanetary shocks by a Fermi mechanism for quasi-parallel shocks (Ellison 1981; Jokipii 1982; Lee 1982) and gradient-drift acceleration (Hudson 1965; Armstrong et al. 1977) for quasi-perpendicular shocks. Quasi-parallel and quasi-perpendicular shocks are so named because the shock normals are quasi-parallel ($\theta_{nB} < 45°$) and quasi-perpendicular ($\theta_{nB} > 45°$) relative to the upstream magnetic fields, respectively (Tsurutani & Lin 1985; Kallenrode 1996). This boundary value of θ_{nB} is, of course, only approximate. For recent reviews of both types of particle acceleration, see Foreman & Webb (1985) and Lee (2000).

Send offprint requests to: S. T. Wu, e-mail: wus@cspar.uah.edu

Particles that are accelerated by a shock, propagate into the upstream (anti-sunward) direction guided by the interplanetary magnetic field. As the shock propagates through interplanetary space, it continuously accelerates energetic particles. During the particle's transport to the point of observation, the particles are subjected to adiabatic deceleration, pitch angle scattering (see Tsurutani et al. 2002), and energy diffusion. Thus, at the spacecraft, the instruments detect particles that have been accelerated at a variety of distances and have undergone different evolution. To compound the problem, the shock itself has evolved (see discussion in Kallenrode 1997a,b) and its particle acceleration efficiency with it. It is the latter problem that we wish to address here by providing the characteristics of shock evolution. Another issue, rarely discussed, is when the shock first forms. We will discuss CME initiation and eventual shock formation.

Although the principles of the physical processes of particle acceleration are reasonably well understood (Lee 2000), we know far less about the shocks themselves. It is not known what physical properties they have at and just after the time of formation (Mach number, M_f, the afore-mentioned θ_{nB} and the upstream plasma β), and how these properties evolve with time and distance. The previously mentioned symbols are defined as follows: M_f is the shock speed (minus the upstream flow speed) divided by the local fast magnetosonic wave speed; and β is the plasma thermal pressure (nkT) divided by the magnetic pressure ($B^2/8\pi$), respectively. Since the onset of the acceleration process may form the "seed particles" for the later acceleration, continued interplanetary acceleration further from the Sun and knowledge of the initiation are extremely important. Different onsets may lead to totally different end results as shown by the empirical results of Heras et al. (1995) who used the early 2D MHD model of Wu et al. (1983) for the temporal shock modelling procedure. This paper is motivated in a similar direction but limited here to the meridional plane.

Recently, Zank et al. (2000) presented a time-dependent model of particle acceleration at a propagating, evolving interplanetary shock. However, their evolving shock model is a kinematic model in which the first principles of the MHD equations are not used. In the present study, our efforts will be to use an 2.5D MHD code to model, for the first time, some of the basic CME-induced and subsequent ICME-induced shock properties from formation near the Sun to 1 AU. We will use a well-studied CME to match measurements at 1 AU (WIND data) in our code to model the CME driven shock.

The shock Mach number, shock normal in the meridional plane, and upstream plasma beta will be modeled as a function of time and distance from the Sun. In addition, the disturbed (downstream) interplanetary parameters at 1 AU will also be presented. There is an important omission in our study, namely the B_ϕ component of the upstream Archimedian spiral interplanetary magnetic field. An appropriate 3D MHD model with full time-dependent boundary conditions at 1 R_s and that extends beyond all critical points (cf. Nakagawa et al. 1987) does not exist as yet. Our self-consistent axisymmetric model includes these boundary conditions and generates B_ϕ as part of the time-dependent solution. However, all partial derivatives with respect to the azimuthal angle, ϕ, are taken to be zero in this present work.

A description of our model is given in Sect. 2. Results are provided in Sect. 3 and some conclusions are noted in Sect. 4.

2. Description of the simulation model for formation of a CME induced shock

To determine shock formation and propagation from the inner solar corona to the heliosphere (~1 AU) due to the propagation of a particular simulated CME, we use a streamer and flux-rope model given by Wu & Guo (1997). The model has been successfully used to model some important features of several CMEs observed by the SOHO spacecraft coronagraph, LASCO (Wu et al. 1997a, 1999, 2000; Plunkett et al. 2000). These CMEs were generated by destabilized streamers and possessed propagating flux-rope magnetic configurations. The mathematical model and procedures used to construct the streamer and flux-rope system were discussed in detail by Wu & Guo (1997) and Wu et al. (1997b) and will not be repeated here. However, to introduce the reader to this topic, a brief description of the model is presented below.

The streamer and flux-rope MHD model consists of a two-flux system oriented orthogonally to each other. One represents a helmet streamer, and the other represents the flux-rope that moves into the computational domain from below the photosphere. Initially, they are in dynamical equilibrium, namely, the quiet solar wind is included. In order to accommodate the additional heating source processes occuring in the solar corona and interplanetary space to match the typical solar wind properties at 1 AU, the polytropic index is chosen to vary with the radial distance from 1.03 to 1.46 (Wu et al. 1999). At the pole the solar wind speed conditions vary from ~10 km s^{-1} at the solar surface to 420 km s^{-1} at 215 (R_s). At the equator, the solar wind varies from 0 km s^{-1} at the solar surface to ~400 km s^{-1} at 215 R_s. There is no solar wind near the sun at the solar equatorial surface because the magnetic field has a closed configuration there (consistent with SOHO observations). Figures 1a and b show the numerically simulated streamer and flux-rope configuration that will serve as the initial background plasma and field. The latter panel, Fig. 1b is the simulated coronagraph white light image.

From top left to bottom right, Figs. 2a and b show the initial state of the following physical parameters: plasma beta, solar wind speed (component in the meridional plane), fast MHD wave speed, slow MHD wave speed, Alfvén speed and sound speed. Different curves within each panel indicate different latitudes as described in the figure title. Figure 2a provides these parameters from 1−10 R_s (i.e. close to the Sun), and Fig. 2b gives a broader perspective out to 220 R_s. These initial parameters are important towards the understanding of CME-induced shock formation, propagation, and relation to the temporally-developing shock properties that are relevant to the efficiency of particle energization. An important characteristic of these parameters given in Fig. 2b can be immediately recognized: that is, these background parameters are not dependent on latitudes beyond ~60 R_s for this particular streamer/solar wind model. In particular, the two

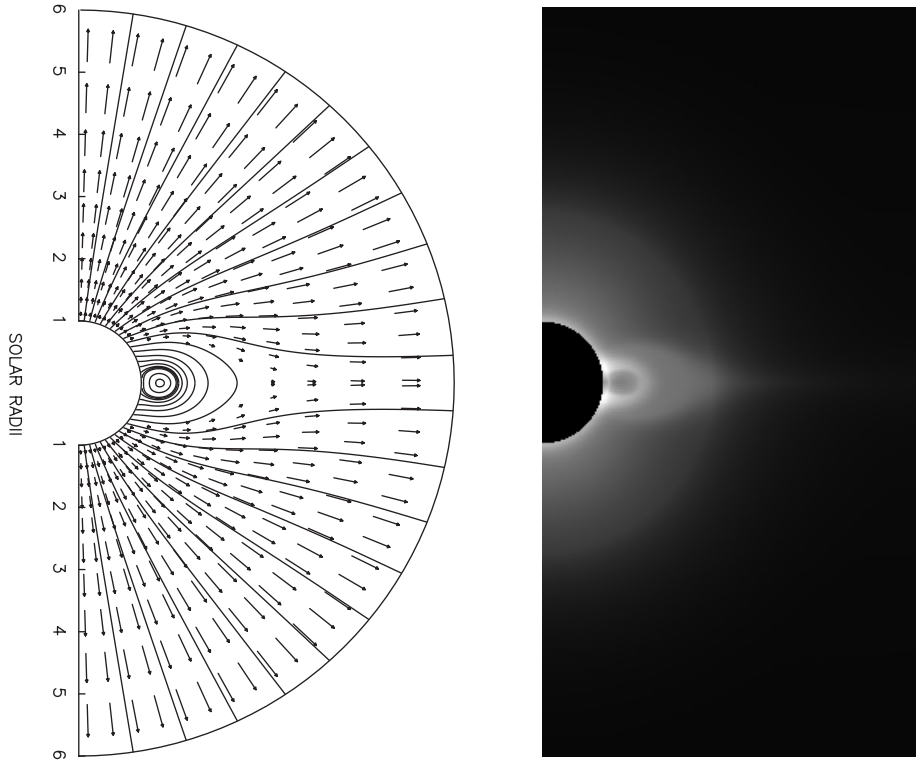

Fig. 1. A representative streamer with magnetic cavity topology where the cavity is formed by a flux-rope with low density and high magnetic field strength; **a)** the magnetic field lines and velocity vectors in the meridional plane; and **b)** the corresponding computed polarization brightness (pB) based on the density distribution of the model (1996). The largest velocity vector at 6 R_s over the pole is ~200 km s^{-1}.

characteristic speeds, fast and Alfvén (plotted in Fig. 2b on a logarithmic scale), indicate that the former is dominated by the latter close to the Sun (Fig. 2a), but is dominated by the sound speed at the larger distances. This behavior, of course, reflects the heliocentric decrease of magnetic energy in the solar wind.

Figure 3 shows the meridional plane plasma beta contours corresponding to the present model of the corona and heliosphere. It is easy to note that the plasma beta is very small ($\ll$1.0) above the coronal holes (open field regions) and is larger over the streamer. We suggest that this variation of β close to the Sun may be relevant to shock-particle energization close to the initial moments of shock formation. We believe that this β variation is important for the following reason; β is inversely proportional to the square of the Alfvén speed for a constant coronal temperature, thus the Alfvénic speed is inversely proportional to the square root of β. In the corona, the value of β is generally much less than unity. This means that the magnetosonic speed is large; consequently, it will affect the formation of shocks.

The analyses of LASCO and the earlier Solar Maximum Mission (SMM) coronal observations (Dere et al. 1997; St. Cyr et al. 1999; Plunkett et al. 2000; Simnett 2000) show that there are many CMEs that are initiated with a streamer and flux-rope magnetic topology. These observations, then, motivated our assumption of this self-consistent, meridional, magnetic configuration (Fig. 1) as the initial state for the launching of a CME. To initiate this simulation, we use the streamer and flux-rope model of Wu & Guo (1997) and introduce an additional component of magnetic field (Wu et al. 1997b) along the radius of the flux-rope (B_ϕ). The mathematical expression to implement this process is:

$$B_\phi^{n+1} = B_\phi^n \left[1 + \gamma\left(1 - \frac{r^*}{0.85 r_f}\right)\right] \quad (1)$$

where r_f is the radius of the flux-rope; γ an arbitrary constant related to the magnitude of increasing field strength, which is chosen to be 0.004 for the present study; r^* the distance between the center of the flux-rope and the point where B_ϕ is added (with $r^* < 0.85\ r_f$); and the superscript, n, indicates the time steps. Physically, this could be interpreted as an injection of magnetic flux along the axis of the filament which, in turn, leads to an increase of current in the radial and meridional directions. This additional current interacts with the background magnetic field and produces an outward Lorentz force ($\boldsymbol{j} \times \boldsymbol{B}$) that destabilizes the streamer, thus launching the CME into interplanetary space (Wu et al. 1999, 2000). The LASCO observations during January 6–12, 1997 (i.e. the so-called January 1997 Sun-Earth Connection interval) is an example of an event of this type. This temporal interval attracted a great deal of attention in the solar-terrestrial community because it was the first time a complete set of data at the solar surface, in interplanetary space, in the magnetosphere and in

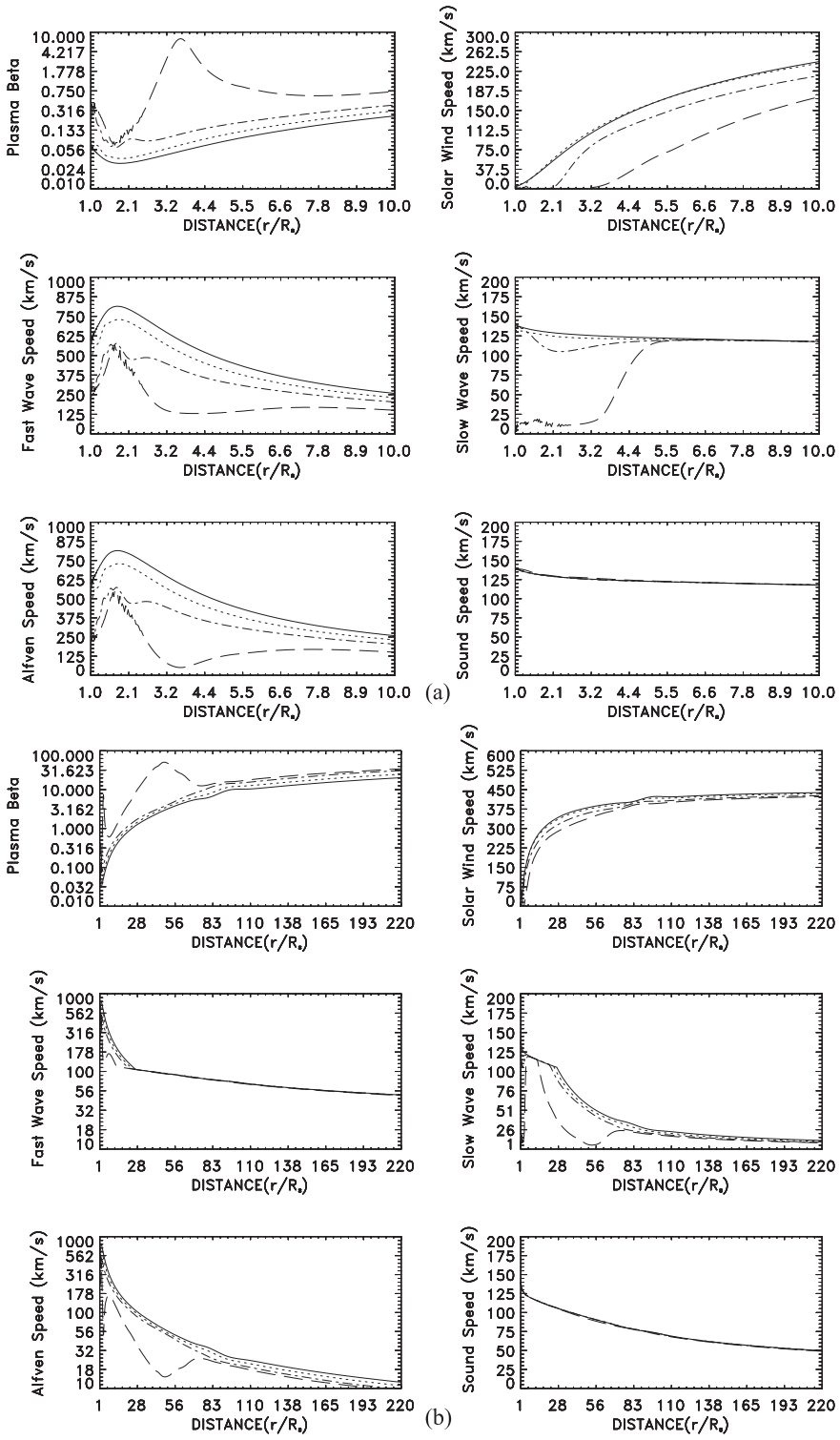

Fig. 2. The initial distribution of plasma beta, solar wind speed, fast wave speed, slow wave speed, Alfvén speed, and sound speed vs. distance from the center of the Sun along four meridional angular directions measured from the north pole. **a)** in the corona and **b)** in the heliosphere. The solid lines = 0° (pole), dotted lines = 45°, dotted-dashed lines = 70°, and dashed lines = 90° (equator).

the ionosphere was recorded. Many in situ solar wind and simulation analyses were presented for this event (Wu et al. 1997c; Burlaga et al. 1998; Lu et al. 1998; Tsurutani et al. 1998). A self-consistent axisymmetric (i.e. 2.5D) MHD analysis of the dynamical relationships between a flux-rope, streamer, coronal mass ejection, and magnetic cloud was presented previously (Wu et al. 1999). In this latter study, Wu et al. (1999) demonstrated that the model simulations were satisfactorily similar to the height-time curves measured by SOHO/LASCO (see Fig. 3b of Wu et al. 1999) and the plasma and magnetic field measured by WIND (see Fig. 9 of Wu et al. 1999). However, the authors did not analyze the CME-induced MHD shock

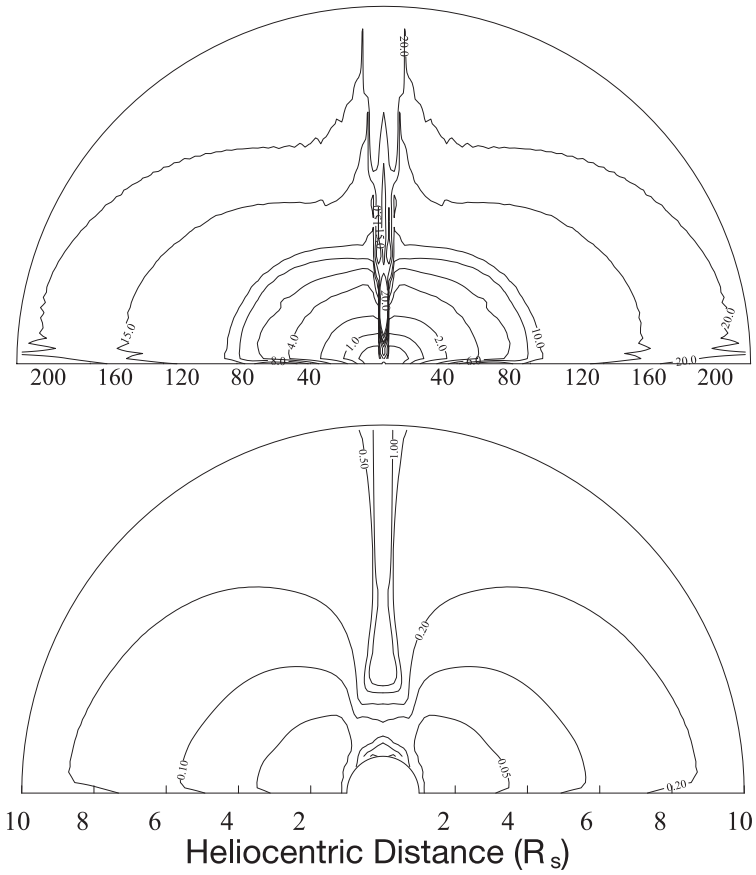

Fig. 3. The initial plasma beta contours: **a)** in the heliosphere (top) and **b)** in the corona (bottom).

developed in the corona and heliosphere. As discussed in the Introduction, the focus of our analysis is an extension of this work. We will discuss the formation of the fast forward shock ahead of the CME, its spatial and temporal propagation through interplanetary space, and some shock properties that may be relevant to the efficiency of particle acceleration during its transition to 1 AU.

3. Results

Figure 4 shows the evolution of the magnetic field and the solar wind velocities in the corona (1−20 R_s) at 1, 3, 5 and 7 hours after the initiation of the CME. The corresponding relative density ($\frac{\rho-\rho_\circ}{\rho_\circ}$) contours are shown in Fig. 5. By examining these two figures together, the formation of the MHD fast shock can easily be identified by the IMF deformation (or kinking) and the steepening density gradient. Approximately one hour after the CME initiation, the MHD fast shock has not yet formed, but the three parts of a frequently-observed CME (Illing & Hundhausen 1986) can be noted in the density profile. The enhanced density legs of the CME can be clearly seen. The density enhancement of the current sheet is also exhibited. Approximately 2 hours after CME initiation, the MHD fast shock first appears (not shown, but can be inferred at t = 3 hrs in the two Figs. 5 and 6). The shock is formed in front of the flux-rope. To identify the MHD shock, we compute the ratio of the wave speed (and its value relative to the background solar wind speed) and fast magnetosonic speed. Since this ratio (fast Mach number, M_f) is greater than unity, we conclude that it is, indeed, a MHD fast shock.

Approximately 5 hrs after initiation (shown in Figs. 4 and 5), the shock front in the equatorial plane (identified by the large velocity vector in Fig. 4 and the high plasma density in Fig. 5) has propagated to a distance of ∼9 R_s from the Sun. The small dimple (i.e., shock speed decrease) in the equatorial plane is caused by the shock's movement into the higher density heliospheric current sheet. At ∼30° above and below the ecliptic, the Mach number of the shock is lower (indicated by the lower kinking of the IMF in Fig. 4) and less compressive (indicated by the density contour diminution in Fig. 5). The shock is also slightly further from the Sun at those angles and at the distance ∼10.5 R_s. At t = 7 hrs, the shock has developed more fully. The shock shape is more symmetric, with the shock occurring at ∼16 R_s from the Sun. As expected, the shock strength is strongest in the ecliptic plane (M_f ∼ 3.5−4) and weaker (M_f ∼ 1.7−2) at higher latitudes.

Figure 6 shows the CME-induced shock wave characteristics. Moving from top to bottom in two columns, (left "corona" and right "heliosphere"), these characteristics include: the radial distance of the shock front from the solar center; the angle of the shock normal relative to the north pole; the downstream (i.e., anti-sunward) plasma beta; and the magnetosonic (fast MHD wave) Mach number as a function of time. The parameters as a function of latitude are given by the four curves in each panel as described in Fig. 6's title. This figure consists

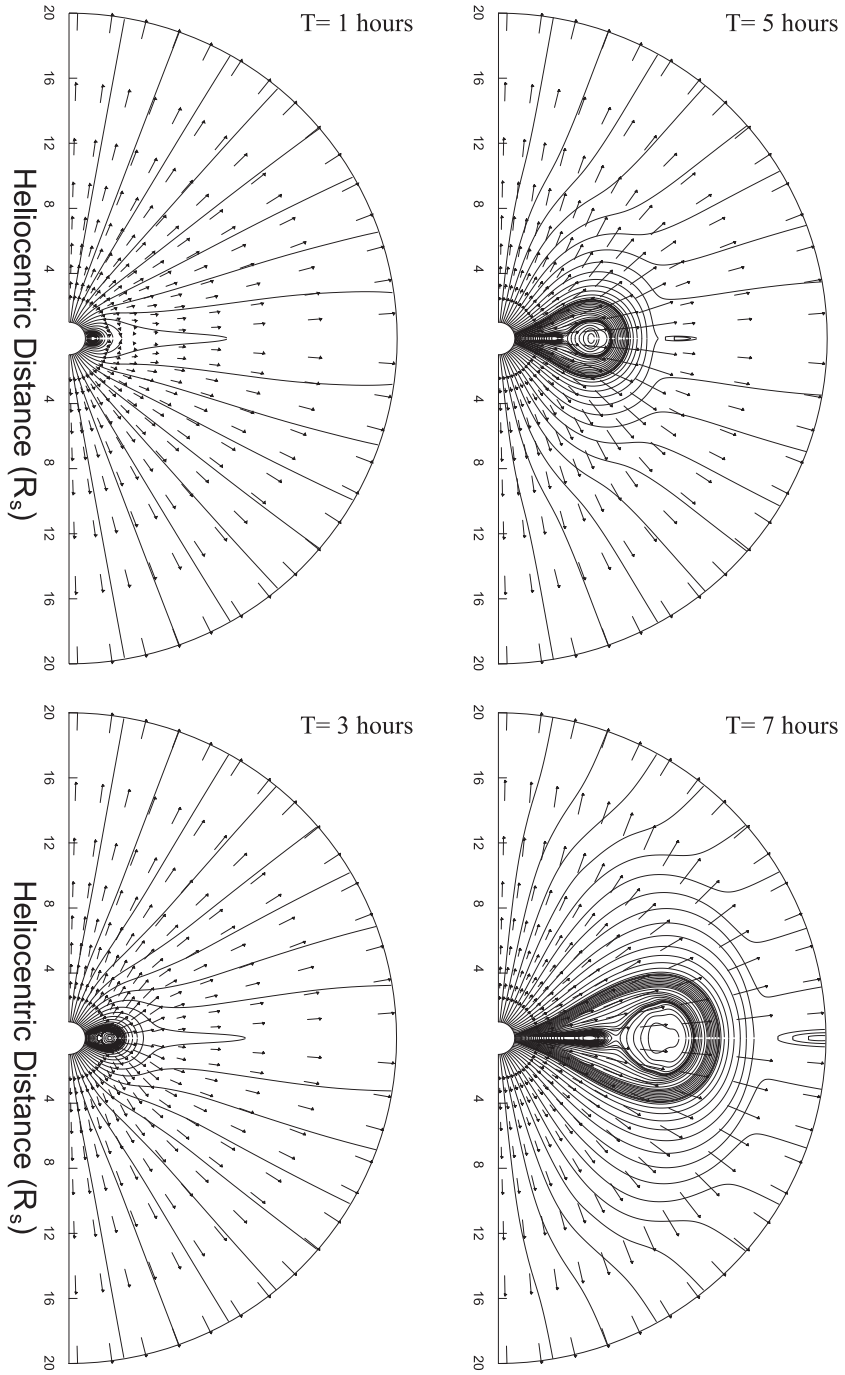

Fig. 4. Magnetic field line and solar wind velocity vectors at times 1, 3, 5, and 7 hours from upper left panel to lower right panel.

of two parts: the left-hand column shows the shock properties in the corona ($1 \leq r \leq 20\ R_s$) and the right-hand column shows the shock properties in the heliosphere ($20 \leq r \leq 220\ R_s$). There are a number of important features found in Fig. 6:

1. The propagation speed of the shock front is highest in the equatorial plane and decreases with increasing (absolute) latitude. This result is to be expected because the motion of the flux-rope (the piston generating the shock), is confined to the equatorial plane.
2. The plasma beta conditions out to 20 R_s, shown in Fig. 7, is much smaller in the polar region than in the equatorial region. This is due to the initial model assumptions that are in accordance with the typical observed properties reported elsewhere. This is also the cause of higher magnetosonic speeds at higher latitudes.
3. The shock magnetosonic (MHD fast wave) Mach number is strongest at the equator and becomes weaker at higher latitudes. For this simulated event (i.e., the Jan. 6–12, 1997 interval), the MHD fast shock first appears ~2 hours (as mentioned above) after CME initiation, at a position of 3.2 R_s from the Sun in the ecliptic plane. The shock Mach number increases with increasing distance from the Sun. A value of $M_f = 3$ is reached at ~18 R_s. The maximum value

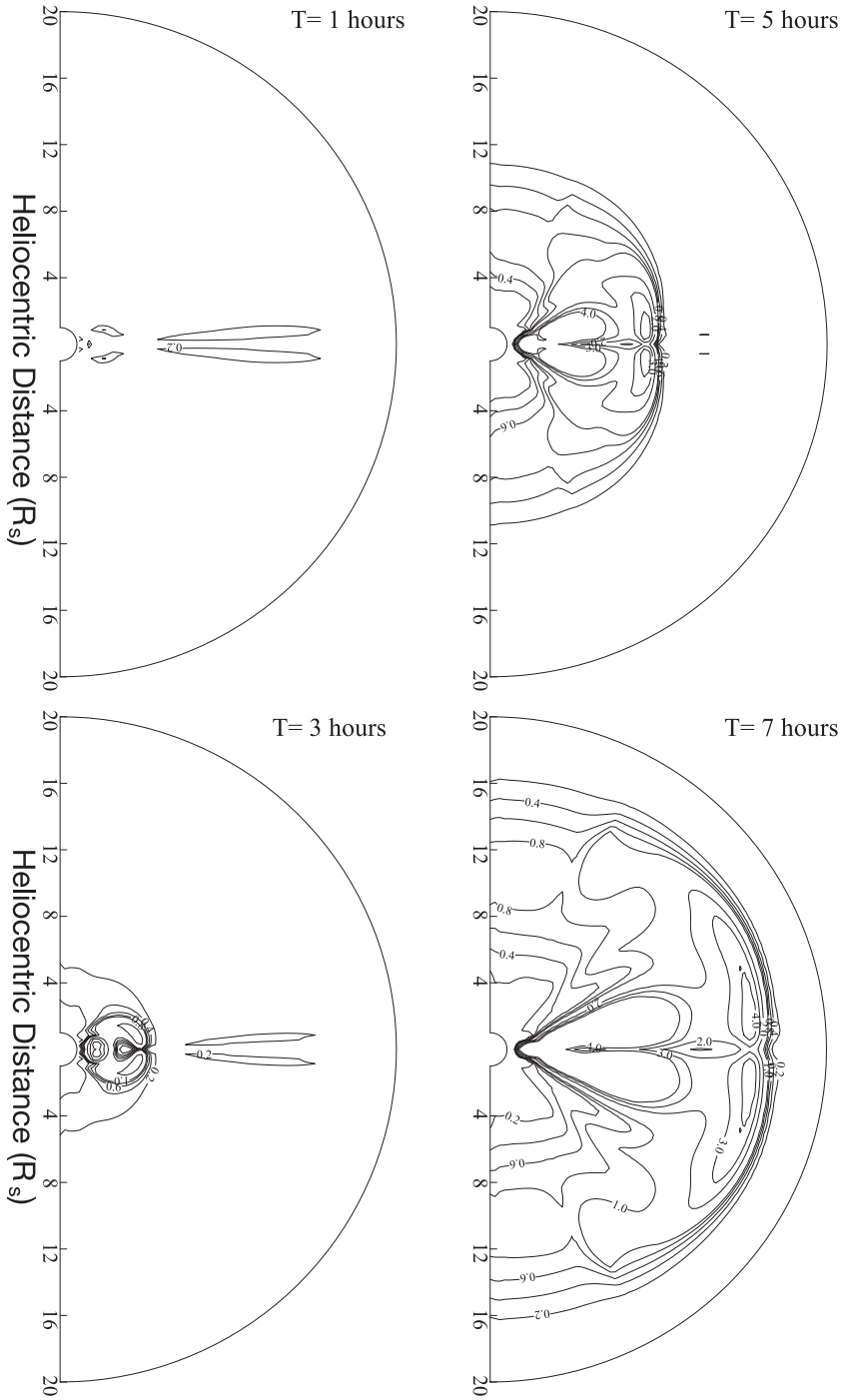

Fig. 5. Density $\frac{\rho-\rho_\circ}{\rho_\circ}$ contours at times 1, 3, 5, and 7 hours from upper left panel to lower right panel.

of $M_f = 4$ occurs at ~130 R_s, then decreases to about 3.5 by 210 R_s (i.e., about 1 AU).

4. The angle of the shock (wave) normal in the meridional plane has its greatest variation at mid-latitudes near the corona. In contrast, the shock normal angle is almost constant at both poles and equator far away from the corona. What is particularly striking is that, beyond 8 to 10 R_s, most of the normal angles on the shock surface remain relatively constant with increasing distance as if we had a uniformly-expanding spherical CME propagation.

To further understand the shock evolution, we have plotted the disturbed (downstream) plasma beta conditions out to 20 R_s shown in Fig. 7. Basically, the coronal plasma is still a low beta plasma except at the streamer where the current sheet is located. The plasma beta increases in the region downstream (i.e. anti-sunward) of the shock. It is also noted that the plasma beta is much smaller within the flux-rope. This latter point is consistent with in situ measurements of magnetic clouds at 1 AU (Klein & Burlaga 1982; Farrugia et al. 1997; Tsurutani & Gonzalez 1997).

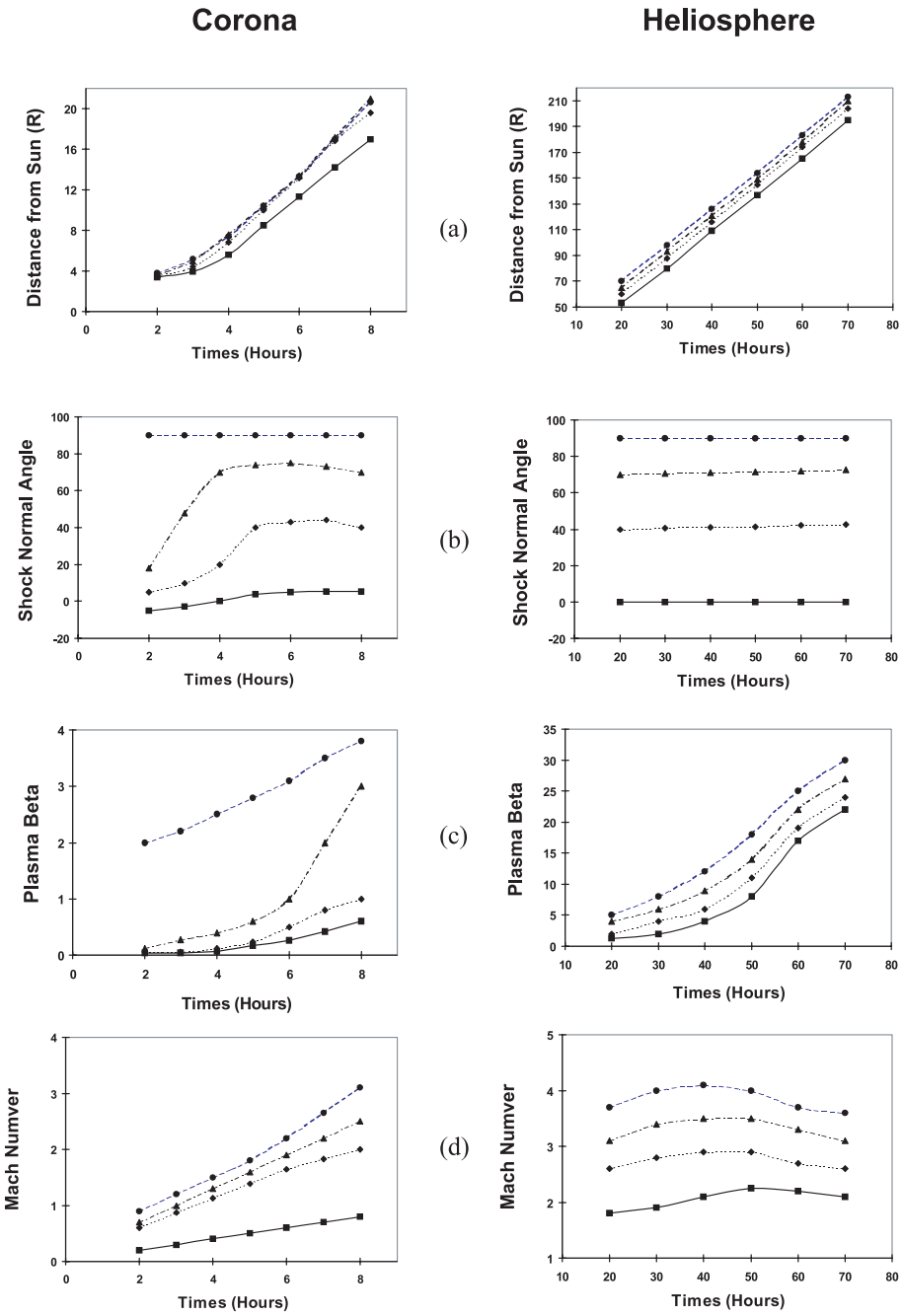

Fig. 6. The left column of panels shows the shock characteristics in the corona (1−30 R_s), and the right column indicates the evolution of these characteristics into the heliosphere (30−212 R_s). **a)** Position of MHD fast wave front; **b)** shock normal angle vs time along four meridional angles measured from the north pole; **c)** plasma beta; and **d)** MHD fast wave Mach number. The solid lines = 0° (pole), dotted lines = 45°, dotted-dashed lines = 70°, and dashed lines = 90° (equator).

We present next the disturbed properties through the shock and the sheath plus magnetic cloud (or ICME): these properties include magnetic fields, velocities, densities and temperatures at 1 AU in detail as a function of time. Figure 8 shows these disturbed properties at the equator in the left panel, and at 45° latitude in the right panel, respectively. In essence, these time series are simulations of what may be observed by appropriately-located spacecraft. The horizontal axis represents hours from CME initiation at the Sun. The first signature that is noted is the fast forward shock at ~70 hrs in the equator and the weaker shock at ~75 hrs at 45° latitude. The shock is indicated by the dashed vertical line denoted by "S". In the equatorial plane, the shock is identified by the rapid jump in velocity from 425 km s^{-1} to ~570 km s^{-1}; temperature from 1.8×10^5 K to 3.1×10^5 K; density from 7 cm^{-3} to 39 cm^{-3}; and magnetic field strength from 1.35 nT to ~32 nT. These physical parameters could also be plotted (not shown here) as a function of radial distance at say, t = 70 hrs, the time shown for the "shock" in Fig. 8. Given the computational grid size at 1 AU to be 1 R_s, 4 grids are required to resolve the shock.

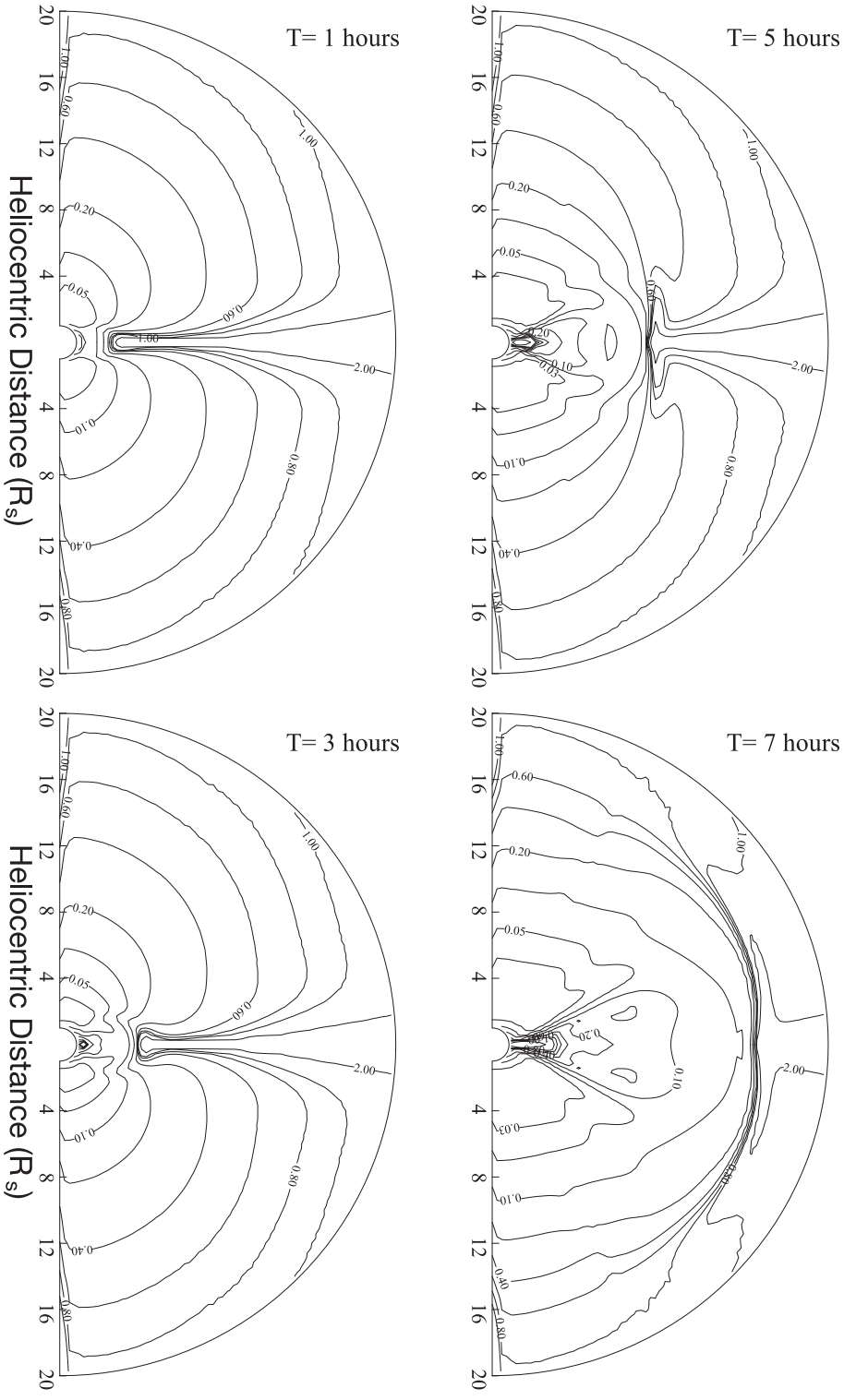

Fig. 7. Plasma beta contours at times 1, 3, 5 and 7 hours from upper left panel to lower right panel.

Thus, the simulated shock jumps might, subjectively, be chosen to be less (using conventional average procedure for "before" and "after" the shock) than those just given from the somewhat coarse temporal resolution in Fig. 8. Furthermore, we have used the analytical solution of Rankin-Hugoniot equations for a spherically-symmetric, 1D, MHD wave propagation model (Han et al. 1982) to verify our numerical results; this procedure shows good agreement for a polytropic index being 1.46. The sheath region (Sh) is just behind the shock and is located between the two vertical dashed lines. It is characterized by high speeds, temperatures, densities and magnetic field strengths. The sheath is the upstream slower solar wind that has now been compressed and swept up by the fast shock.

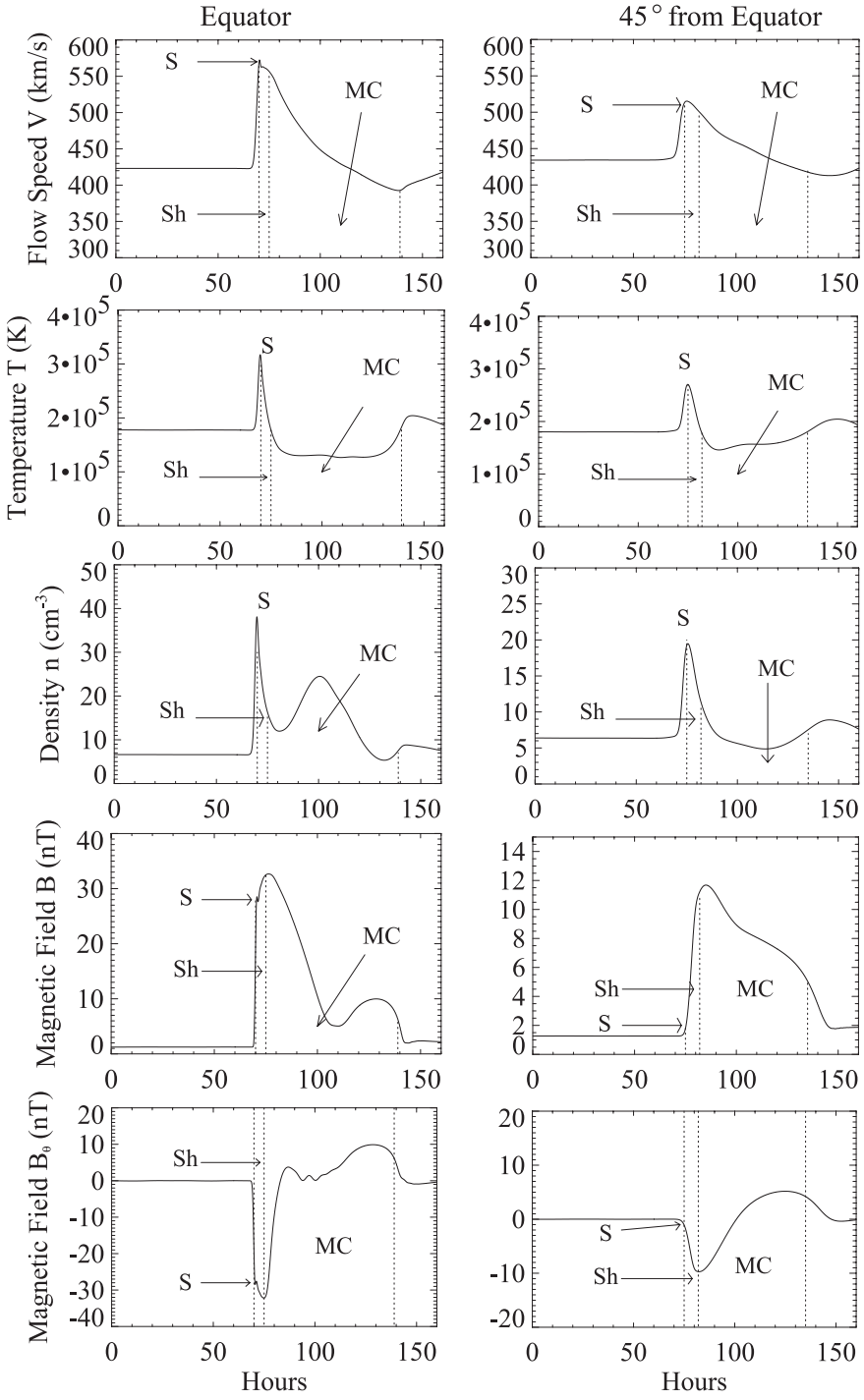

Fig. 8. The disturbed velocity, density, temperature, total magnetic fields, and latitudinal components (B_θ) at 1 AU as a function of time at the equator (left panel) and 45° away from the equator (right panel), respectively, where S, Sh and MC indicate the shock, sheath, and magnetic cloud.

Following the sheath is the magnetic cloud (MC). This region is identified by the higher solar wind density (~27 cm^{-3} maximum) at the equator; low temperature (1.3×10^5 K) and high field strengths. The β value within the cloud is the lowest of any of the regions shown. The magnetic cloud B_θ values show a characteristic south-north turning.

The characteristics of the interplanetary event at 45° latitude are similar to those in the ecliptic, but with subtle and important differences. The shock at higher latitudes is weaker and delayed from that in the ecliptic plane, as mentioned previously. This means that the shock has taken a slight "bullet" shape, a deviation from a spherical shape. The maximum in the velocity is only ~520 km s^{-1}, less than at the nose of the event (~570 km s^{-1}). The temperature (2.7×10^5 K) and density (20 cm^{-3}) of the sheath plasma is much less than in the ecliptic plane because of the relatively weaker shock strength at the higher latitudes. The magnetic field strength reaches a maximum value of only ~11 nT.

The magnetic cloud is much less well defined in temperature and density. However, it is much better defined in field magnitude and B_θ, giving the appearance that one often finds in interplanetary space for some ICMEs that are referred to as magnetic clouds.

The additional magnetic compressional features noted in the ecliptic plane (and not present at high latitudes) are due to the driven nature of the flux-rope. It should be noted that the turning direction of B_θ depends on the field polarity chosen for the model. The latter would be directly related to the observations of the solar magnetic field at the photospheric level. In the present simulation, we have chosen a north-south bipole streamer. That is why the resulting simulation exhibits a B_θ southward turning first and then northward turning. If the initial field polarity were south-north, then the resulting magnetic field would be in reverse order from the present case. It is interesting to note that Guo et al. (1996) showed, from this streamer and flux-rope configuration, that the streamer polarity determines the interplanetary magnetic field (IMF) configuration at 1 AU (because of the magnetic reconnection process). This implies that, when the flux-rope has a polarity opposite to that of the streamer, through reconnection, the flux-rope will be converted to the streamer's polarity. In other words, the IMF response depends on the streamer's configuration rather than that of the flux-rope. On a slightly different note, see also comments on energetic particle transport through sector boundaries, Kallenrode (1993).

4. Conclusion

We have simulated a coronal shock formation and its propagation and evolution from the Sun to the heliosphere using a self-consistent axisymmetric MHD flux-rope model (Wu & Guo 1997; Wu et al. 1999). A flux-rope emergence into a streamer from below the photosphere was assumed for the driver of the CME. We find that the CME was nonlinearly accelerated close to the Sun. The shock is formed very close to the Sun, at a distance of ~3.2 R_s from its surface, in the ecliptic plane. The shock Mach number reaches a maximum value of 4 at 130 R_s, and at 1 AU, the Mach number is slightly reduced to ~3.5.

By examining the results shown in Figs. 4, 5, and 7 together, it is recognized that the flux-rope served as a piston for the generation of a MHD fast shock. For example, the highly compressed region shown in the density distribution (Fig. 5) is ahead of the flux-rope, i.e., the region sometimes called the CME sheath (Tsurutani et al. 1998). In this region, the plasma beta is larger than it is within the flux-rope as shown in Fig. 7. The shock is formed only when the speed of the CME driver relative to the upstream plasma is faster than the local magnetosonic speed. Because the magnetosonic speed near the sun is very high (low β plasma), shock formation is prohibited until the CME reaches 3.2 R_s.

In summary, we have presented a self-consistent, global axisymmetric (i.e. 2.5D) MHD model with an initial state consisting of a streamer and flux-rope imbedded in a model solar wind. We have demonstrated that the model is capable of predicting the location, strength and normal of the CME induced shock. By comparing the model results and typical observed characteristics, we immediately noted that the filament plasma mass is missing after the magnetic cloud. This is because our model only includes the flux-rope as a proxy of the magnetic cloud without filament structure within the flux-rope.

We suggest that the shock conditions (cf., M_f and absolute magnetic field and velocity jumps) along the global shock configuration are, as suggested by Heras et al. (1995) and others, relevant to any study of the efficiency of shock energization processes. These parameters can be found only by MHD simulation such as demonstrated by this example. However, we have not demonstrated the θ_{nB} calculation that must await a fully three-dimensional MHD simulation.

There has been a great deal of discussion about which occurs first, the release of a CME or the onset of a solar flare (Harrison 1986; Hundhausen 1999; Sveskta 1995; Dryer 1996). Much of the debate stems from the extrapolation of observations of the CME high in the corona back to the site of origin. These arguments have dealt with small time differences of minutes up to tens of minutes. In this paper, we have shown that it takes hours from the time of the release/initiation of a slow CME to the formation of a shock upstream of the CME. Our model results on the acceleration of the CMEs in the lower corona are in very good agreement with the coronagraph measurements of SOHO (cf., Wu et al. 1999), so we can feel quite confident about the accuracy of the model. The implications are quite important for the origin of solar flare particles. Clearly the CME shock that we discuss in this paper can accelerate particles only well after the CME has propagated to 3.2 R_s and beyond. The shock will have only a Mach 1.0 speed at this distance, and will gain strength at a later time and distance as it propagates into the lower magnetic field strength and density environment. Thus, solar flare particles that arrive at 1 AU within a few hours of the flare/CME launch cannot be due to acceleration by a CME shock mechanism of the particular class discussed here. Another mechanism(s) must be responsible. Some suggestions are included in the magnetic reconnection process (Sakai & de Jager 1996; Podgorney & Podgorney 2001) occurring near the flare site. We suggest that solar flare particle scientists compare and contrast these first-arriving (prompt) particle properties to those (gradual enhancements) detected in situ at the ICME shock proper to help understand the differences/similarities of the two mechanisms.

Fast CMEs, on the other hand, have been found to have exponential speed profiles that peak within 2−3 R_s with high constant speeds in the upper corona (Shanmugaraju et al. 2003, and references therein). These fast CMEs will most certainly exceed the local magnetosonic speed (and form a shock) closer to the Sun than slow CMEs, but how much closer and how much faster is beyond this current effort. We plan on following the present paper with a subsequent work which will model and follow the fast CME shock formation from the lower corona to 1 AU. Just as there are two types of CMEs, there will be two different types of shock formation sequences and also two types of associated particle events.

There are, of course, variations in the speeds of slow CMEs and fast CMEs. This will lead to variations in the CME shock properties giving a spectrum of delay times in shock formaton, time delays of the shock reaching maximum Mach numbers,

etc. In our future efforts we will examine SOHO CME observations to attempt to estimate the variability of shock formation and shock evolution as a function of time and distance from the Sun based on our modeling results.

As a final remark, we would like to point out that the initial interplanetary magnetic field topology has not included the Parker spiral field. Thus the model-predicted shock normals have been measured only in the meridional plane relative to the north pole. However, the model-predicted shock normals in the inner heliosphere (20 R_s) are believed to be accurate because the open magnetic field lines are almost radial.

Overall, this model has demonstrated the capability to give quantitative descriptions of the undisturbed and disturbed physical parameters of simulated CME shocks that propagate from the Sun to the near Earth environment. The next step is to couple the predicted shocks and their shocked plasma properties to develop a more complete (Tsurutani & Lin 1985; Heras et al. 1995; Lario, et al. 1998; Zank et al. 2000) particle acceleration model. The model can then be tested with observed SEP events.

Acknowledgements. Work performed by STW and TXZ was supported by Air Force AFOSR F49520-00-0-0204, National Science Foundation ATM 0070385 and ATM 0316115, NASA NAG5-12843, and Jet Propulsion Laboratory via Engineering International Inc. Portions of this work were performed (BT) at the Jet Propulsion Laboratory, Calif. Inst. Tech under contract with NASA. MD was supported by a NASA LWS contract NAG5-12527 via Exploration Physics International, Inc. The authors also wish to thank Dr. M.-B. Kallenrode for her helpful comments on the manuscript.

References

Armstrong, T. P., Chen, G., Sarris, E. T., & Krimigis, S. M. 1977, in Study of Travelling Interplanetary Phenomenon, ed. M. A. Shea, D. F. Smart, & S. T. Wu (Massachusetts: D. Reidel), 367
Burlaga, L. F., Fitzenreiter, R., Lepping, R., et al. 1998, JGR, 103, 277
Cane, H. V., McGuire, R. E., & von Rosenvinge, T. T. 1986, ApJ, 301, 448
Dere, K., Brueckner, G. E., Howard, R. A., et al. 1997, Sol. Phys., 175, 601
Dryer, M. 1996, Sol. Phys., 169, 421
Ellison, D. C., Monte Carlo 1981, Simulation of Collisionless Shock Acceleration, Ph.D. Thesis (Washington, DC: The Catholic Univ. of Amer.)
Farrugia, C. J., Burlaga, L. F., & Lepping, R. P. 1997, in Magnetic Storms, ed. B. T. Tsurutani, W. D. Gonzalez, Y. Kamide, & J. K. Arballo (Washington, DC: Amer. Geophys. Union Press), 98, 91
Forman, M. A., & Webb, G. M. 1985, in Collisionless Shocks in the Heliosphere: A Tutorial Rev., ed. R. G. Stone, & B. T. Tsurutani, 34, 91
Guo, W. P., Wu, S. T., & Tandberg-Hanssen, E. 1996, ApJ, 469, 944
Han, S. M., Wu, S. T., & Nakagawa, Y. 1982, Compters and Fluids, 10, 8, 159
Harrison, R. A. 1986, A&A, 162, 283
Heras, A. M., Sanahuja, B., Lario, D., et al. 1995, ApJ, 445, 497
Hudson, P. D. 1965, MNRAS, 131, 23
Hundhausen, A. J. 1999, in The Many Faces of the Sun, ed. K. Strong, J. L. R. Saba, B. M. Haisch, & J. T. Schmelz (New York: Springer-Verlag), 143
Illing, R. M. E., & Hundhausen, A. J. 1986, JGR, 91, 10951
Jokipii, J. R. 1982, ApJ, 255, 716
Kallenrode, M.-B. 1993, JGR, 98, 5573
Kallenrode, M.-B. 1996, JGR, 101, 24393
Kallenrode, M.-B. 1997a, JGR, 102, 22347
Kallenrode, M.-B. 1997b, JGR, 102, 22335
Kahler, S. W., Sheeley, Jr., N. R., Howard, R. A., et al. 1984, JGR, 89, 9683
Klein, L. W., & Burlaga, L. F. 1982, JGR, 87, 613
Lario, D., Sanahuja, B., & Heras, A. M. 1998, ApJ, 509, 415
Lee, M. A. 1982, JGR, 87, 5063
Lee, M. A. 2000, in Acceleration and Transport of Energetic Particles Observed in the Heliosphere: ACE 2000 Symp., ed. R. A. Mewaldt, J. R. Jokipii, M. A. Lee, E. Möbius, & T. H. Zurbuchen, Amer. Inst. Phys., 3
Lin, R. P. 1987, Rev. Geophys. 25, 676
Lu, G. D., Baker, D. N., McPherron, R. L., et al. 1998, JGR, 103, A6, 11685
McGuire, R. E., von Rosenvinge, T. T., & Reames, D. V. 1984, JGR, 89, 9683
Nakagawa, Y., Hu, Y. Q., & Wu, S. T. 1987, A&A, 179, 354
Plunkett, S. P., Vourlidas, A., Simberova, S., et al. 2000, Sol. Phys., 194, 371
Podgorney, A. I., & Podgorney, I. M. 2001, Astron. Rep., 45, 60
Reames, D. V. 1995, Rev. Geophys. Suppl. 585
Reames, D. V. 1999, Space Sci. Rev., 90, 413
Sakai, J.-I., & de Jager, C. 1996, Space Sci. Rev., 77, 1
Shanmugaraju, A., Moon, Y.-J., Dryer, M., & Umapathy, S. 2003, Sol. Phys. 215, 185
Simnett, G. M. 2000, J. Atmosph. Solar-Terres. Phys., 62, 1423
St. Cyr, O. C., Burkepile, J. T., Hundhausen, A. J., & Leeinski, A. R. 1999, JGR, 104, 12 493
Svestak, Z. 1995, Sol. Phys. 160, 53
Tsurutani, B. T., & Lin, R. P. 1985, JGR, 90, 1
Tsurutani, B. T., Gonzalez, W. D., Tang, F., Akasofu, S.-I., & Smith, E. J. 1988, JGR, 93, 8519
Tsurutani, B. T., & Gonzalez, W. D. 1997, in Magnetic Storms, ed. B. T. Tsurutani, W. D. Gonzalez, Y. Kamide, & J. K. Arballo (American Geophys. Union Press), 98, 77
Tsurutani, B. T., Arballo, J. K., Lakbina, G. S., et al. 1998, JGR, 25, 3047
Tsurutani, B. T., Zhang, L. D., Mason, G. L., et al. 2002, Annales Geophysicae, 20, 427
Wu, S. T., Dryer, M., & Han, S. M. 1983, Sol. Phys., 84, 395
Wu, S. T., & Guo, W. P. 1997, Geophysical Monograph Series, 99, ed. N. Crooker, J. Joselyn, & J. Feynman (Washington, DC: AGU), 83
Wu, S. T., Guo, W. P., Andrews, M. D., et al. 1997a, Sol. Phys., 175, 719
Wu, S. T., Guo, W. P., & Dryer, M. 1997b, Sol. Phys., 170, 265
Wu, S. T., Guo, W. P., Michels, D. J., et al. 1997c, in Proc. 5th SOHO Workshop, ESA SP-404, The Corona and Solar Wind Near Minimum Activity, 739
Wu, S. T., Guo, W. P., Michels, D. J., & Burlaga, L. F. 1999, JGR, 104, A7, 14789
Wu, S. T., Guo, W. P., Plunkett, S. P., Schmieder, B., & Simnett, G. M. 2000, J. Atmosph. Solar-Terres. Phys., 62, 1489
Zank, G. P., Rice, W. K. M., & Wu, C. C., 2000, JGR, 105,(A11), 25079